ACS OMEGA

http://pubs.acs.org/journal/acsodf

Article

Solid−Liquid Phase Equilibrium of Ammonium Dihydrogen Phosphate and Agricultural Grade Ammonium Polyphosphate (Degree of Polymerization Ranging from 1 to 8) for Mixed Irrigation Strategy

Xiaohou Zhou, Dejun Xu, Dehua Xu, Zhengjuan Yan, Zhiye Zhang, Benhe Zhong, and Xinlong Wang*

Cite This: *ACS Omega* 2022, 7, 35885−35900

Read Online

ACCESS | Metrics & More | Article Recommendations | Supporting Information

ABSTRACT: Water-soluble ammonium polyphosphate (APP) has the advantages of good solubility and slow-release characteristics and has the potential to be used in combination with monoammonium phosphate (MAP) as a high phosphorus content slow-release fertilizer to improve the utilization rate of phosphorus during irrigation. Herein, the effects of the APP1 concentration and temperature (278.2−313.2 K) on the solubility of MAP, solution density, and pH value in the ternary equilibrium system (APP1−MAP−water) were measured. The simplified Apelblat model, two empirical polynomials, and rational two-dimensional functions can describe the experimental solubility data, solution density, and pH value well, respectively, with reliable modeling parameters (R^2 > 0.99). In the OptiMax1001 reactor, the focused beam reflectance measurement (FBRM), the particle-view measurement (PVM), and the ReactIR 15 probes were used to observe and reverse verify that they can be synergistically codissolved to achieve economic efficiency. Basic thermodynamic data and models can guide their collaborative application in irrigation to improve the phosphorus utilization rate.

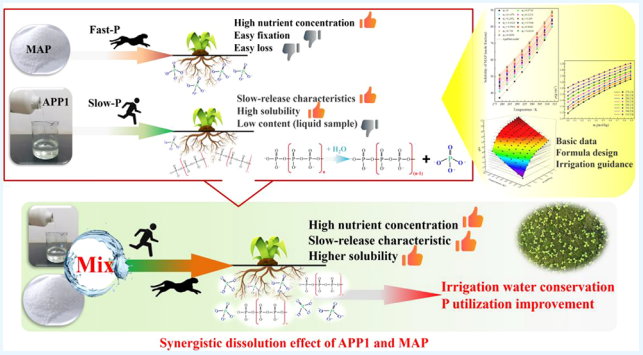

1. INTRODUCTION

Water-soluble ammonium polyphosphate (APP) can be used for water-soluble fertilizers with the advantages of good solubility, strong compatibility, low crystallization temperature, and good chelation performance.[1] APP with different degrees of polymerization had significant differences in solubility and hydrolysis rate. The dissolved APP can be slowly converted into orthophosphate by hydrolysis, which can be used by crops. This slow-release behavior of phosphorus nutrition was beneficial to improve the utilization rate of phosphorus. At present, agricultural APP products are mostly mixtures of ammonium polyphosphate with different degrees of polymerization. The distribution of polymerization degree of agricultural APP products directly affected its agricultural application value,[2] thus promoting the continuous improvement of its production technology.[3] Hossner and Freeouf demonstrated that APP can react with the manganese fertilizer to produce $Mn_3(NH_4)_2(P_2O_7)_2{\cdot}H_2O$ in soil.[4] Hill et al. concluded that the P mobility of monoammonium phosphate (MAP) in the soil column was lower than APP.[5] The research results of Venugopalan and Prasad showed that the wider the distribution of the degree of polymerization of water-soluble APP, the higher the utilization rate of phosphorus in crops.[6] Xie et al. established a method for the determination of water-soluble APP with different degrees of polymerization distribution.[7] The research results of Gao et al. showed that the application of water-soluble APPs with different polymerization degrees into soil could significantly increase the content of soil-available phosphorus and the availability of soil trace elements.[8] The research results of some scholars from China pointed out that water-soluble APP achieved good effects as a fertilizer on corn, tomato, loofah, watermelon, and other crops and played a role in increasing the yield and improving the crop quality.[9] Thus, as a good slow-effect phosphate fertilizer raw material, APP can be combined with traditional fertilizer materials to improve phosphorus utilization.[10]

Industrial-grade MAP is an important raw material of water-soluble fertilizers with high phosphorus content, and ammonium ion can promote the uptake of phosphorus by plants. However, the available phosphorus provided by MAP cannot be fully absorbed and utilized by crops in a short period of time and

Received: July 19, 2022
Accepted: September 13, 2022
Published: September 26, 2022

https://doi.org/10.1021/acsomega.2c04534
ACS Omega 2022, 7, 35885−35900

Table 1. Reagents Used in This Study

material[a]	CAS Reg. no.	supplier	mass fraction[b]	purification method	analytical method
MAP	7722-76-1	Chendu Jinshan Chemical Co., Ltd.	≥0.995	drying	quinoline phosphomolybdate gravimetric method[16]
APP1	68333-79-9	GuangXi Yueyang Chemical Co., Ltd	≥0.600	filtering	ion chromatography[17]
deionized water	7732-18-5	laboratory preparation	≥0.999	none	none

[a]MAP, monoammonium phosphate ($NH_4H_2PO_4$); APP1, ammonium polyphosphate solution ($(NH_4)_{n+2}P_nO_{3n+1}$); resistivity of water used in this study was 18.25 MΩ•cm. [b]Declared by the supplier.

Table 2. Character of APP1

raw material[a]	Mn (g/mol)	N %	P_2O_5%	H_2O %	WAP	NAP	PR	PDI
APP1[b]	271	11.1	37.4	41.13	3.59	2.54	89.3	1.41

[a]WAP, average polymerization by weight; NAP, number average degree of polymerization; PR, polymerization rate; PDI, polymer dispersity index. [b]Declared by the supplier.

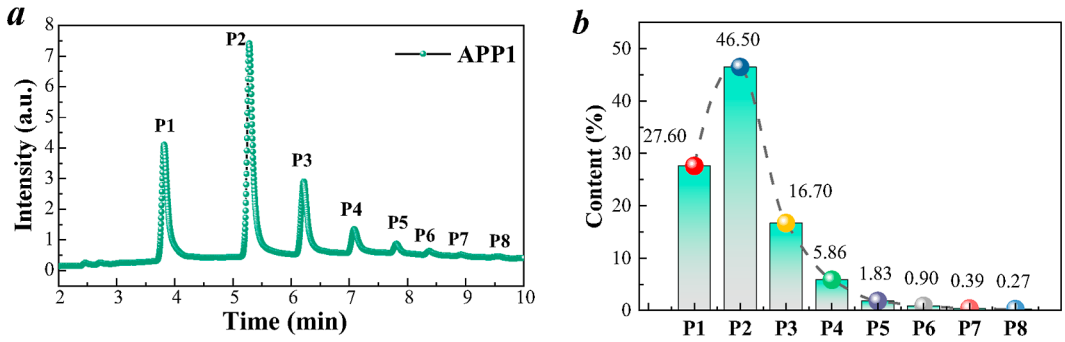

Figure 1. Phosphorus species composition analysis in APP1: (a) Ion chromatographic analysis and (b) analysis of relative contents of different phosphorus species.

is easily lost or fixed in the deep soil. On this basis, MAP can be mixed with different fertilizer products to achieve nutrient diversity and pursue functionality and efficiency. Relevant studies have explored the solid−liquid equilibrium law of various substances codissolved with MAP in order to explore the optimal fertilizer allocation scheme and basic data. Xu et al. measured the solubilities of MAP in the systems of $(NH_4)_2SO_4$−water and NH_4F−water at the temperatures of 293.2 and 343.2 K.[11] Yang et al. determined the solubility and density data in the ternary system of urea phosphate + ammonium dihydrogen phosphate + water at 25 and 55 °C to conduct corresponding phase diagrams.[12] Srinivasan et al. studied the mutual solubility and metastable zone width of ammonium dihydrogen phosphate and potassium dihydrogen phosphate (KDP) to open up the application prospect for the mixing of MAP and KDP as fertilizers in agriculture.[13] Zhumaniyazov et al. analyzed the determination results of solubility in ternary system $(CH_2)_6N_2$−MAP−water in a wide temperature range to expand fertilizer application programs.[14] In addition, APP is a slow-P species with sufficient P−O−P structure, which can not only show the chelating effect of impurity ions but also realize the slow-release effect of orthophosphate (ortho-P) through hydrolysis. Therefore, the combination of agricultural MAP and APP irrigation can provide both quick-available P and slow-available P for crops and even achieve better cosolubility. As good fertilizer products, they have a good potential for mixed use, but the study on phase balance of this mixing system is still lacking.[15] In this study, APP1 used was a liquid water-soluble fertilizer with special degree of polymerization distribution, and the solubility of MAP was determined by the dynamic method in the ternary solution system under different conditions. Considering the regional differences between north and south China, the temperature condition was set as 278.2−313.2 K to cover the environmental conditions that fertilizers may be exposed to during actual use. For economic reasons, we focused on the study of the system in which P_2O_5 provided by APP1 was less than 30% of the total P_2O_5, so the dosage range of APP1 was controlled within 0.8856 mol/kgH_2O during the experiment of mixed dissolution of APP1 and MAP. The reason for choosing water as the solvent was to simulate the real situation of agricultural irrigation. The density and pH values of the solid−liquid equilibrium solution were captured simultaneously. Reliable parametric models were established for all obtained thermodynamic data to guide the formulation. Furthermore, confirmatory experiments were designed to test the effect of APP1 on supersaturated MAP, combined with online detection techniques of ReactIR 15, focused beam reflectance measurement (FBRM), and particle-view measurement (PVM) in an OptiMax 1001 reactor.

2. EXPERIMENTAL SECTION

2.1. Materials. The reagents used in the experiments are listed in Table 1. All of the solid salt reagents were dried to a constant weight at 383.2 K before using. Deionized water was employed in all experiments. A kind of ammonium polyphosphate solution with a well-defined composition of phosphorus species was used as the raw material.[18] APP1 is a water-soluble liquid fertilizer consisting of ammonium pyrophosphate, ammonium tripolyphosphate, ammonium pentaphosphate, and other forms, and the content of ammonium pyrophosphate is the highest. The composition and properties of APP1 are shown in Table 2 and Figure 1. The polymer dispersity index (PDI) value of APP1 was higher than 1.0, indicating that it can release phosphorus more slowly with

https://doi.org/10.1021/acsomega.2c04534
ACS Omega 2022, 7, 35885−35900

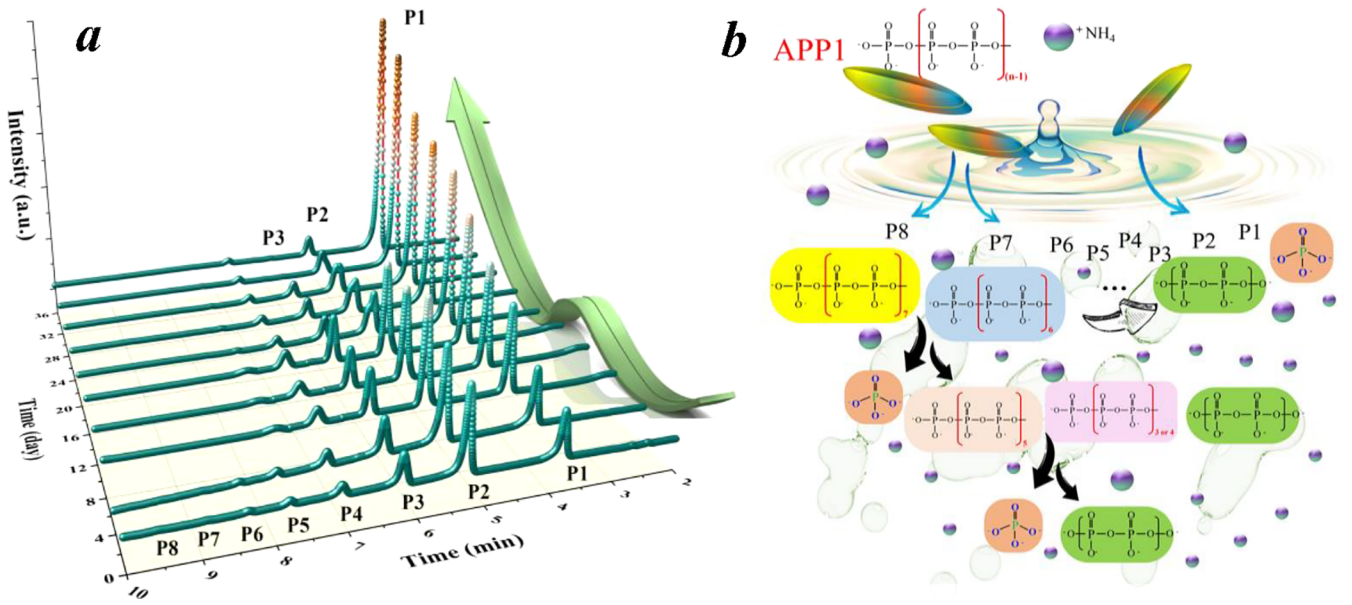

Figure 2. Dissolution of APP1 in water and sustained release of nutrients: (a) Variation of polymerization degree distribution with time in APP1 solution. (b) Schematic diagram of the slow release of nutrients in APP1 solution. Photograph courtesy of Xiaohou Zhou. Copyright 2022. Used with permission.

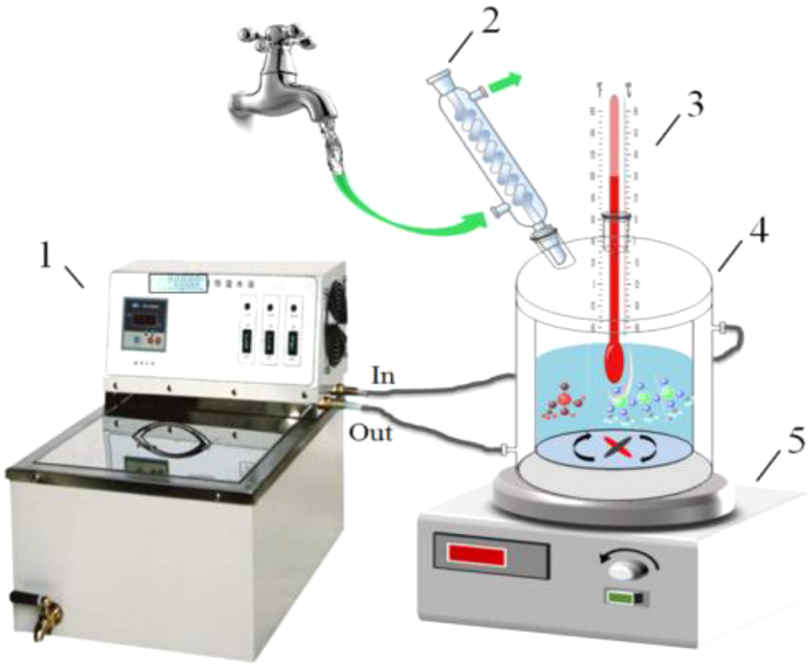

Figure 3. Experimental apparatus for the solubility measurement: (1) Thermostatic bath; (2) condensing return pipe; (3) mercury thermometer; (4) jacketed glass vessel; (5) magnetic stirring. Photograph courtesy of Xiaohou Zhou. Copyright 2022. Used with permission.

hydrolysis reaction in soil.[19] Previous studies showed that the wider the distribution of the degree of polymerization of water-soluble APP, the higher the utilization rate of phosphorus for crops.[20] Thus, APP1 can be used in combination with MAP to provide fast- (fast-P) and slow- (slow-P) available phosphorus for crops. All APP1 was used for experiments within 3 days after being produced, and APP1 was stored at 271.2 K to avoid hydrolysis and to ensure the stability of raw material properties.

In Figure 1a, the ion chromatographic peaks from P1 to P8 successively represented phosphate ions in different forms of phosphorus polymerization from PO_4^{3-} to P_8O_{25}.[10−21] Figure 1b points the specific composition of different phosphorus species which can act as fast phosphorus and slow phosphorus in the fertilizer application process to improve phosphorus utilization.

Figure 2a summarizes the changes of phosphorus species in the APP1 solution system at 298.2 K over time. Within 4 days, little change in phosphorus species composition was caused by polyphosphate hydrolysis in the system. Therefore, the phase equilibrium experiment of the mixed dissolution of MAP and APP1 was completed within 3 h, and the possible kinetic effects of the hydrolysis process could be ignored. After 8 days, P8, P7, P6, and P5 peaks gradually disappeared, while the P1 peak increased significantly. This indicates that phosphorus in higher

https://doi.org/10.1021/acsomega.2c04534
ACS Omega 2022, 7, 35885−35900

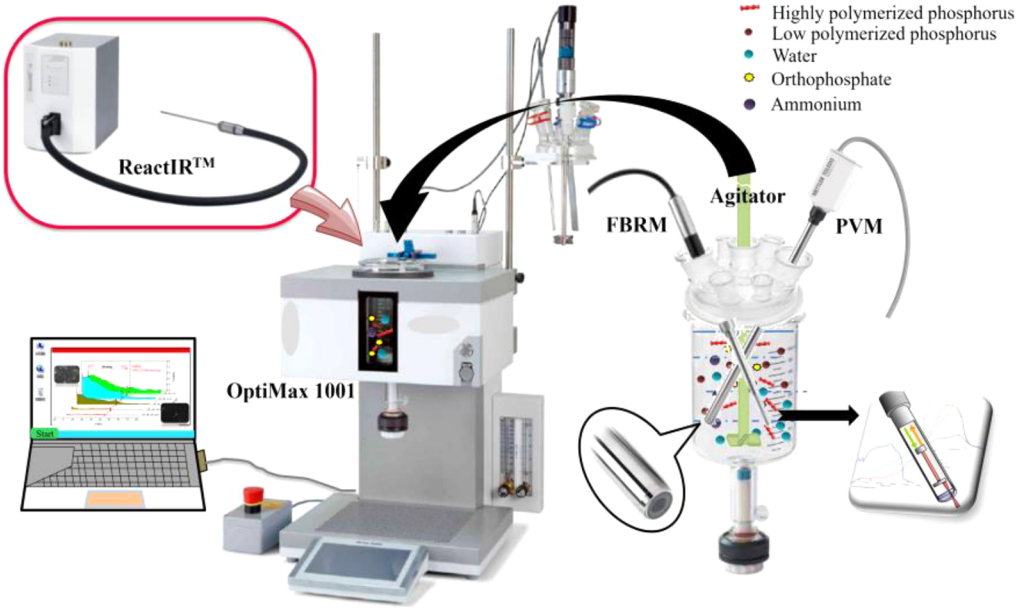

Figure 4. Monitoring device for MAP and APP1 mixed dissolution process. Photograph courtesy of Xiaohou Zhou. Copyright 2022. Used with permission.

polymerization states of APP1 is slowly hydrolyzed into $P_2O_7^{4-}$ and PO_4^{3-} and then absorbed and utilized by farmland crops.[22] As shown in Figure 2b, APP dissolved into water to release NH_4^+, PO_4^{3-}, $P_2O_7^{4-}$, $P_3O_{10}^{5-}$, $P_4O_{13}^{6-}$, $P_5O_{16}^{7-}$, $P_6O_{19}^{8-}$, $P_7O_{22}^{9-}$, and $P_8O_{25}^{10-}$. The polyphosphate ions all tended to be slowly converted into PO_4^{3-} through hydrolysis reaction over time.

2.2. Apparatus and Measurement of Solubility. The solubility of MAP was determined by a dynamic method in the ternary APP1−MAP−water system to analyze the influence of water-soluble APP1.[23] In this work, the experimental apparatus for the measurement of solubility was composed of a low-temperature constant temperature reaction bath, a magnetic stirrer, a jacket reactor, a precision thermometer, and a condensing tube, as depicted in Figure 3. All experiments were performed in the same laboratory, and the ventilation device was dynamically controlled to ensure the pressure stability of the experimental environment.

In the experiment, the magnetic stirrer was maintained until the end of the experiment to keep homogeneous mixing, and the temperature in the jacket reactor was controlled by the low-temperature constant temperature reaction bath through circulating water. First, a certain concentration of water-soluble APP1 solution was prepared and added to the jacket reactor, whose temperature was controlled by the reaction bath to reach the set value. Then, each time a small amount of MAP, which had been accurately measured, was added to this solution until the last addition of MAP was insoluble or not completely dissolved in the final solution. The undissolved MAP particles could still be observed with the naked eye after 30 min, indicating that the system had reached a new equilibrium. In this established solid−liquid equilibrium system, the solubility at the set temperature was calculated by the total addition of MAP. All solubility measurements of APP1 and MAP in the ternary system were carried out under different addition ratios of APP1 at different temperature conditions. The molar content (x_1) of water-soluble APP1 and the molar content (x_2) of MAP were calculated as follows

$$x_1 = \frac{m_1/M_1}{\frac{m_1}{M_1} + \frac{m_0}{M_0}} \quad (1)$$

$$x_2 = \frac{m_2/M_2}{\frac{m_1}{M_1} + \frac{m_0}{M_0} + \frac{m_2}{M_2}} \quad (2)$$

where m_1, m_2, and m_0 are the masses of water-soluble APP1, MAP, and water in the APP1−MAP−water system in turn; M_1, M_2, and M_0 are, respectively, the molar masses of APP1, MAP, and water.

In addition, the pH value and density of the solutions were measured by a pH meter and a 50 mL density bottle, respectively. Before each measurement, we needed to calibrate the pH meter with two standard buffer solutions and ensure that the temperature of the tested solution was the same as that of the calibration solution. The electrode was immersed in the solution to be measured and stirred evenly until a stable pH value was read. The density bottle was calibrated by injecting deionized water cooled after boiling into the density bottle and measuring the density value under different constant temperature conditions (same as the solubility measurement experiment). Two parallel measurements were carried out under each temperature condition to ensure that the difference between the two measurements is not greater than 0.01 g/cm^3. Density bottles were thoroughly cleaned and dried before use, and bubbles should be avoided during measurement. With the addition of water-soluble APP1, the density calculation formula of the solution system was as follows

$$\rho = (m_a - m_b)/V \quad (3)$$

where m_a is the mass of the density bottle full of the solution, m_b is the mass of the density bottle, and V is the volume of the density bottle. A precision thermometer of 0.01 K was used to monitor the temperature of the solution all the time, and an electronic balance with a precision of 0.0001 g was used to precisely weigh the samples. Then, the liquid-phase composition changes were analyzed by ion chromatography and in situ infrared spectroscopy, and the solid phase was analyzed by XRD

https://doi.org/10.1021/acsomega.2c04534
ACS Omega 2022, 7, 35885−35900

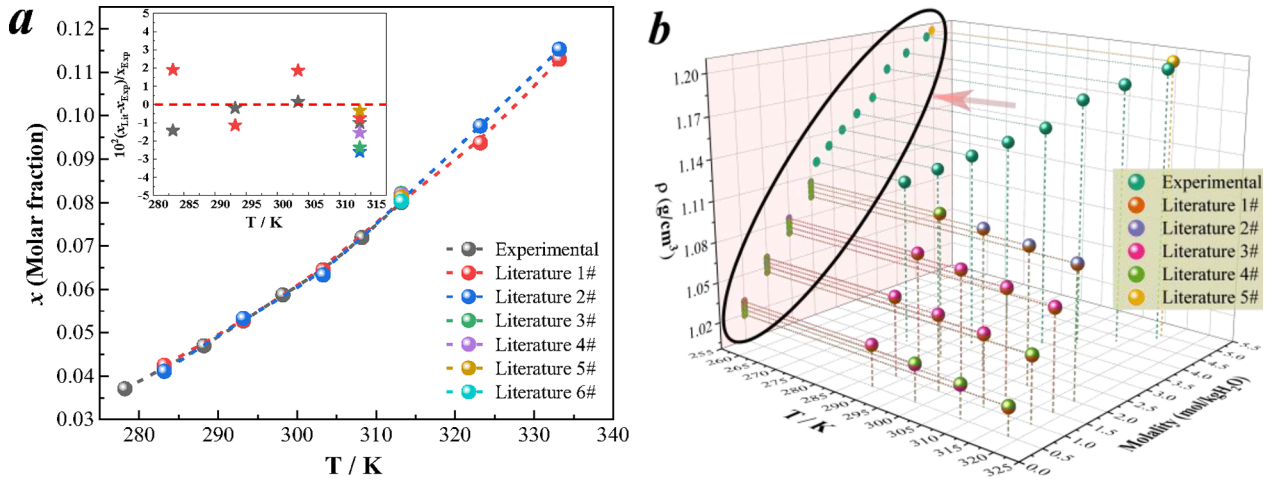

Figure 5. Comparison of literature and experimental data: (a) Solubility of MAP in water: literature 1# ref 27, Copyright 2016 American Chemical Society, literature 2# ref 28, Copyright 1920 Elsevier, and literature 3#, 4#, 5#, 6# ref 29, Copyright 2017 Elsevier. (b) Density of MAP solution: literature 1# ref 30, Copyright 1984 American Chemical Society, literature 2# ref 31, Copyright 2017 American Chemical Society, literature 3# ref 32, Copyright 2019 American Chemical Society, literature 4# ref 33, Copyright 2021 Elsevier, and literature 5# ref 29, Copyright 2017 Elsevier. Used with permission.

after full drying at 303.2 K. The measurement experiments were repeated three times to ensure accuracy and consistency of final results.

The reliability of the conclusion of phase equilibrium law of the three-phase system was verified by observing the mixed dissolution process of APP1 and MAP with an online detection system. The OptiMax 1001 reactor can provide stable temperature change and a stirring environment.[24] FBRM was used to track and record the real-time changes of the number of different particles in the system.[25] The gradual reduction of particles in this system meant that the particles were gradually dissolved, and this change of particle number was recorded by FBRM in real time. When it was observed that the number of particles in the system decreased to 0, it could be considered that all solids were completely dissolved, that is, the change curve of the number of particles collected by FBRM completely coincided with the *X* axis. Meanwhile, the real-time microscopic images of the system were collected by PVM,[26] which can also intuitively record the change of particles in the system. The experimental device is given in Figure 4.

3. RESULT AND DISCUSSION

First, the solubility of MAP in water and the density of the saturated solution were measured. Each group of experiments was repeated three times to ensure reliable results. The evaluation method of uncertainty for all reported quantities is described in detail in the Supporting Information. All experimental data were compared with the literature data in Figure 5 and are tabulated in Tables S1 and S2. It can be seen that the solubility data obtained in this work were in good agreement with the literature data, and the relative deviations were all less than 2.6%. In addition, although the concentration interval of MAP solution measured in the literature did not coincide with that in this paper, the consistency of data change trend can be seen through the mapping projection analysis. Therefore, these results indicated that the experimental method adopted in this paper was reliable.

3.1. Effect of APP1 Addition on the Solubility of MAP.

Within the measured temperature range, the molarities (m_1, m_2) and molar fractions (x_1, x_2) of APP1 and MAP in the equilibrium state are listed in Table 3. We define the ratio of orthophosphate phosphorus content to total phosphorus content in the liquid phase at equilibrium state as OT to reflect the composition ratio of fast-available phosphorus and slow-available phosphorus in the system, and the corresponding calculation formula is as follows

$$\mathrm{OT} = \frac{P_2O_{5\ (\mathrm{Ortho-P})}\%}{P_2O_{5\ (\mathrm{total})}\%} \times 100\% \quad (4)$$

where $P_2O_{5(\mathrm{Ortho\text{-}P})}$ % refers to the phosphorus content in the form of orthophosphate ions, while $P_2O_{5(\mathrm{total})}$ % is the total phosphorus content in the liquid phase. $P_2O_{5(\mathrm{Ortho\text{-}P})}$ % and $P_2O_{5(\mathrm{total})}$ % in the liquid phase were measured by a SEAL AA3 auto continuous-flow analyzer and an inductively coupled plasma-optical emission spectrometer (PE Optima 7000), respectively.

As can be seen from Table 3, the solubility of MAP was positively correlated with the temperature and the concentration of APP1 in the three-phase co-dissolution system. At the same temperature, the solubility of MAP increased with the increase of APP1 addition. For example, at 293.2 K, the solubility of MAP in pure water was 3.0890 mol/kgH_2O, while the solubility of MAP increased to 3.7891 mol/kgH_2O when APP1 addition reached 0.6642 mol/kgH_2O with an increment of 22.66%. When the addition of APP1 was controlled at 0.6642 mol/kgH_2O, the solubility of MAP at 313.2 K was 1.405 times that at 293.2 K. Moreover, it should be emphasized that the measured solubility (mole fraction) of MAP at 313.2 K was 80.0497, while the solubility of MAP can only reach 80.0498 when adding a small amount of APP1 (0.07380 mol/kg). At a relatively high temperature, the solubility of MAP had been significantly improved, and only a small amount of APP1 had little effect on the solubility of MAP. This situation intuitively led to the illusion that the solubility curves in Figure 9a appeared to be close to crossover.

The experiment was repeated at 313.2 K with an APP1 dosage of 0.8856 mol/kgH_2O, and the liquid phase infrared spectroscopy data of the system were recorded in real time using the ReactIR15 probe. From 10 to 50 min, 120.03 g of APP1 was slowly added into 500.13 mL of deionized water to prepare

https://doi.org/10.1021/acsomega.2c04534
ACS Omega 2022, 7, 35885−35900

Table 3. Solubility of MAP and pH and Density Value of the Equilibrium System at Various APP1 Concentrations with Temperature Range from 278.2 to 313.2 K and at Pressure p = 0.1 MPa[a,b]

m_1 (mol/kgH_2O)	m_2 (mol/kgH_2O)	ρ (g/cm^3)	pH	10^3x_1	10^3x_2	OT
			278.2 K			
0.0000	2.1430	1.12	4.03	0.0000	37.1411	1.0000
0.0738	2.3650	1.13	4.34	1.3267	40.7791	0.9663
0.1476	2.4400	1.15	4.53	2.6498	41.9658	0.9410
0.2214	2.4990	1.15	4.65	3.9694	42.8829	0.9146
0.2952	2.5710	1.16	4.74	5.2856	44.0080	0.8937
0.3690	2.6199	1.17	4.82	6.5982	44.7510	0.8801
0.4428	2.6914	1.18	4.87	7.9075	45.8579	0.8635
0.5166	2.7447	1.19	4.95	9.2132	46.6648	0.8417
0.5904	2.7956	1.20	5.00	10.5156	47.4300	0.8310
0.6642	2.8640	1.21	5.03	11.8145	48.4736	0.8204
0.7380	2.9355	1.22	5.08	13.1100	49.562	0.8121
0.8118	2.9999	1.22	5.12	14.4021	50.5309	0.8003
0.8856	3.0458	1.23	5.15	15.6908	51.2013	0.7687
			283.2 K			
0.0000	2.4272	1.13	3.93	0.0000	41.8605	1.0000
0.0738	2.6427	1.14	4.20	1.3267	45.3507	0.9716
0.1476	2.7249	1.16	4.40	2.6498	46.6369	0.9574
0.2214	2.7871	1.16	4.53	3.9694	47.5914	0.9309
0.2952	2.8585	1.17	4.63	5.2856	48.6884	0.9134
0.3690	2.9085	1.18	4.70	6.5982	49.4371	0.9000
0.4428	2.9943	1.19	4.77	7.9075	50.7564	0.8892
0.5166	3.0397	1.20	4.81	9.2132	51.4236	0.8699
0.5904	3.0967	1.21	4.85	10.5156	52.2722	0.8604
0.6642	3.1633	1.21	4.89	11.8145	53.2693	0.8412
0.7380	3.2272	1.22	4.93	13.1100	54.2195	0.8308
0.8118	3.2968	1.23	4.97	14.4021	55.2554	0.8229
0.8856	3.3451	1.24	5.00	15.6908	55.9512	0.8137
			288.2 K			
0.0000	2.7397	1.14	3.83	0.0000	46.9976	1.0000
0.0738	2.9172	1.15	4.09	1.3267	49.8272	0.9741
0.1476	2.9979	1.17	4.29	2.6498	51.0707	0.9600
0.2214	3.0656	1.17	4.42	3.9694	52.0976	0.9415
0.2952	3.1285	1.18	4.52	5.2856	53.0437	0.9259
0.3690	3.1903	1.19	4.60	6.5982	53.9676	0.9123
0.4428	3.2768	1.20	4.66	7.9075	55.2808	0.9023
0.5166	3.3169	1.21	4.70	9.2132	55.8511	0.8873
0.5904	3.3765	1.22	4.74	10.5156	56.7266	0.8757
0.6642	3.4457	1.22	4.78	11.8145	57.7503	0.8631
0.7380	3.5285	1.23	4.84	13.1100	58.9832	0.8601
0.8118	3.5803	1.24	4.88	14.4021	59.7233	0.8512
0.8856	3.6346	1.24	4.92	15.6908	60.5003	0.8438
			293.2 K			
0.0000	3.0890	1.15	3.73	0.0000	52.6728	1.0000
0.0738	3.2667	1.17	3.96	1.3267	55.4660	0.9839
0.1476	3.3431	1.17	4.16	2.6498	56.6189	0.9645
0.2214	3.4158	1.18	4.29	3.9694	57.7058	0.9535
0.2952	3.4731	1.19	4.40	5.2856	58.5445	0.9382
0.3690	3.5489	1.20	4.47	6.5982	59.6725	0.9250
0.4428	3.6235	1.21	4.54	7.9075	60.7753	0.9137
0.5166	3.6677	1.22	4.57	9.2132	61.3945	0.9019
0.5904	3.7129	1.22	4.61	10.5156	62.0275	0.8914
0.6642	3.7891	1.23	4.65	11.8145	63.1420	0.8828
0.7380	3.8710	1.24	4.71	13.1100	64.3399	0.8744
0.8118	3.9162	1.25	4.76	14.4021	64.9635	0.8719
0.8856	3.9811	1.25	4.79	15.6908	65.8887	0.8623
			298.2 K			
0.0000	3.4655	1.16	3.65	0.0000	58.7168	1.0000
0.0738	3.6040	1.18	3.88	1.3267	60.8444	0.9837
0.1476	3.6771	1.19	4.06	2.6498	61.9252	0.9716

https://doi.org/10.1021/acsomega.2c04534
ACS Omega 2022, 7, 35885−35900

Table 3. continued

m_1 (mol/kgH_2O)	m_2 (mol/kgH_2O)	ρ (g/cm^3)	pH	10^3x_1	10^3x_2	OT
			298.2 K			
0.2214	3.7585	1.19	4.19	3.9694	63.1302	0.9549
0.2952	3.8072	1.20	4.30	5.2856	63.8170	0.9427
0.3690	3.8894	1.21	4.37	6.5982	65.0248	0.9365
0.4428	3.9431	1.22	4.46	7.9075	65.7831	0.9214
0.5166	3.9764	1.22	4.48	9.2132	66.2199	0.9145
0.5904	4.0235	1.23	4.51	10.5156	66.8702	0.9022
0.6642	4.0978	1.24	4.56	11.8145	67.9375	0.9011
0.7380	4.2045	1.24	4.62	13.1100	69.4983	0.8925
0.8118	4.2257	1.25	4.66	14.4021	69.7392	0.8842
0.8856	4.2874	1.26	4.70	15.6908	70.5998	0.8769
			303.2 K			
0.0000	3.8276	1.18	3.46	0.0000	64.4561	1.0000
0.0738	3.9731	1.19	3.79	1.3267	66.6608	0.9856
0.1476	4.0526	1.20	3.94	2.6498	67.8193	0.9730
0.2214	4.1213	1.20	4.09	3.9694	68.8055	0.9643
0.2952	4.1719	1.21	4.19	5.2856	69.5058	0.9567
0.3690	4.2570	1.22	4.27	6.5982	70.7358	0.9453
0.4428	4.2953	1.23	4.35	7.9075	71.2400	0.9336
0.5166	4.3491	1.23	4.39	9.2132	71.9796	0.9279
0.5904	4.3975	1.24	4.44	10.5156	72.6338	0.9177
0.6642	4.4724	1.25	4.49	11.8145	73.6899	0.9105
0.7380	4.5780	1.25	4.56	13.1100	75.2078	0.9012
0.8118	4.6031	1.26	4.60	14.4021	75.4970	0.8942
0.8856	4.6681	1.27	4.64	15.6908	76.3901	0.8902
			308.2 K			
0.0000	4.3068	1.19	3.36	0.0000	71.9452	1.0000
0.0738	4.3571	1.20	3.70	1.3267	72.6340	0.9885
0.1476	4.4298	1.21	3.87	2.6498	73.6661	0.9767
0.2214	4.5113	1.21	3.99	3.9694	74.8288	0.9660
0.2952	4.5489	1.22	4.09	5.2856	75.3129	0.9588
0.3690	4.6383	1.23	4.17	6.5982	76.5870	0.9575
0.4428	4.6700	1.24	4.25	7.9075	76.9753	0.9432
0.5166	4.7296	1.24	4.28	9.2132	77.7871	0.9383
0.5904	4.7899	1.25	4.32	10.5156	78.6057	0.9271
0.6642	4.8877	1.25	4.36	11.8145	79.9850	0.9271
0.7380	4.9913	1.26	4.43	13.1100	81.4439	0.9153
0.8118	5.0247	1.27	4.47	14.4021	81.8463	0.9096
0.8856	5.0965	1.27	4.52	15.6908	82.8191	0.9075
			313.2 K			
0.0000	4.8342	1.20	3.36	0.0000	80.0497	1.0000
0.0738	4.8406	1.21	3.62	1.3267	80.0498	0.9913
0.1476	4.8665	1.22	3.77	2.6498	80.3457	0.9840
0.2214	4.9565	1.22	3.89	3.9694	81.6105	0.9746
0.2952	4.9801	1.23	4.00	5.2856	81.8684	0.9656
0.3690	5.0867	1.24	4.08	6.5982	83.3733	0.9582
0.4428	5.1191	1.25	4.16	7.9075	83.7587	0.9499
0.5166	5.1490	1.25	4.18	9.2132	84.1050	0.9472
0.5904	5.2072	1.26	4.21	10.5156	84.8720	0.9369
0.6642	5.3228	1.27	4.24	11.8145	86.4901	0.9324
0.7380	5.4282	1.27	4.30	13.1100	87.9463	0.9259
0.8118	5.4714	1.28	4.35	14.4021	88.4787	0.9207
0.8856	5.5373	1.28	4.40	15.6908	89.3417	0.9175

[a]Standard uncertainties u are $u(T) = 0.2$ K, $u(P) = 0.5$ kPa; relative standard uncertainties are $u_r(m) = 0.0100$, $u_r(x) = 0.0100$, $u_r(\rho) = 0.01$, u_r(pH) = 0.01, and u_r(OT) = 0.0100. [b]m_1 and m_2, molalities of APP1 and MAP, respectively; x_1 and x_2, mole fractions of APP1 and MAP, respectively; OT, ratio of orthophosphate phosphorus content to total phosphorus content.

APP1 solution. After 50 min, referring to the results in Table 3, a total of 318.53 g of MAP (5.5373 mol/kgH_2O) was gradually added to the solution in batches, and the changes of particles in the system were monitored by FBRM during the whole process. After the last MAP addition at 96 min, FBRM was used to observe for more than 30 min until no solid particles larger than 1 μm were observed, indicating that the system reached equilibrium (around 114 min). As shown in Figure 6a, the

https://doi.org/10.1021/acsomega.2c04534
ACS Omega 2022, 7, 35885−35900

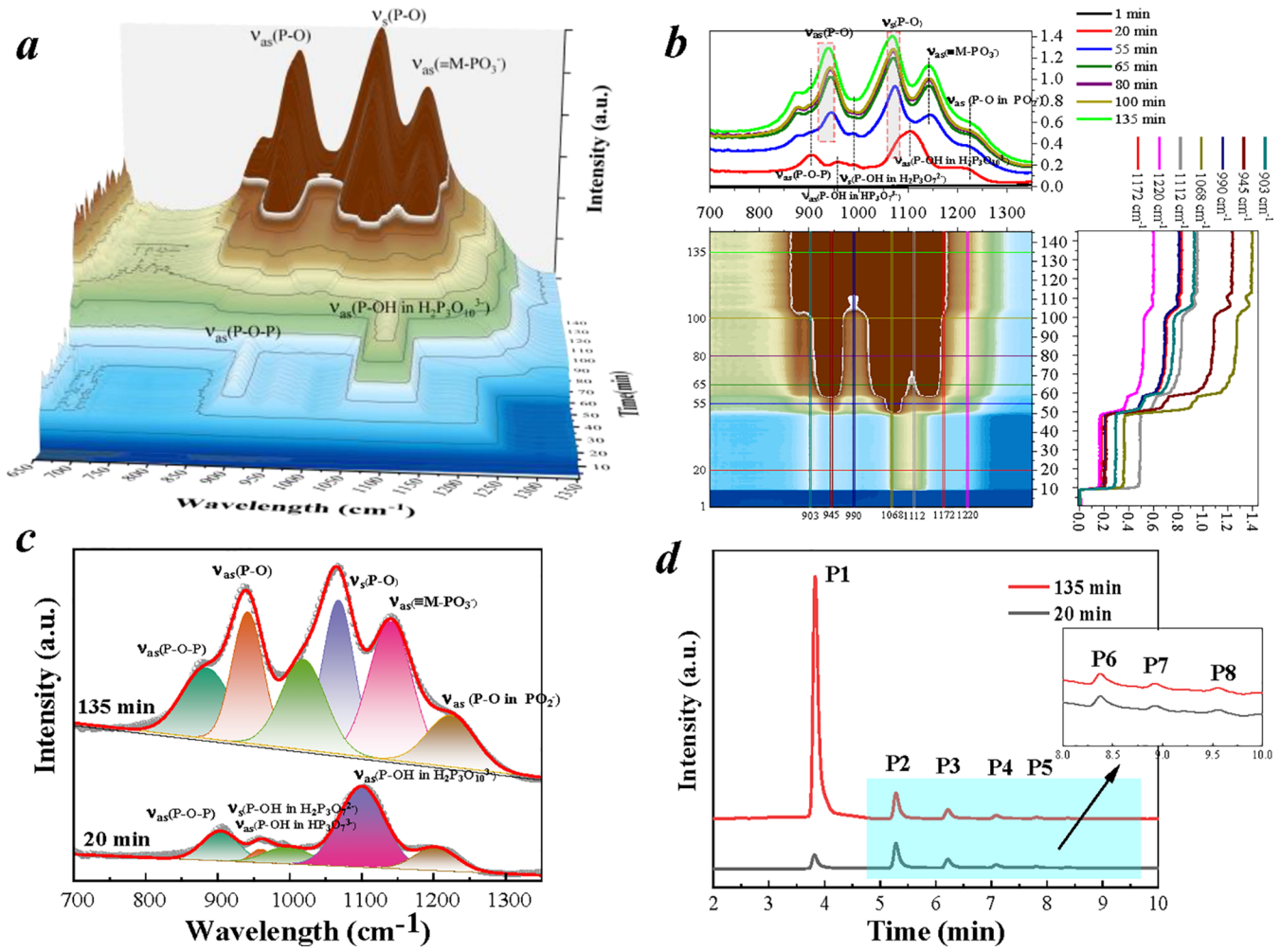

Figure 6. In situ liquid-phase infrared spectroscopy data of APP1−MAP−water system (a−c) and IC analysis (d).

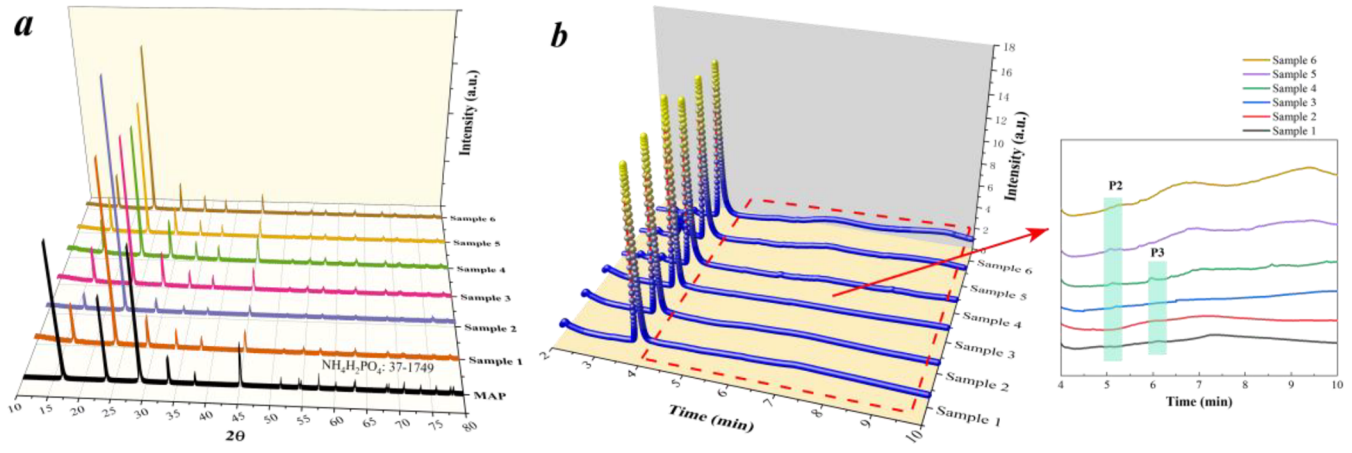

Figure 7. Solid-phase composition analysis: (a) XRD pattern. (b) Ion chromatography phosphorus species analysis.

results of IR spectrum were used to analyze the composition change of the liquid-phase system and the hydrolysis of polyphosphate. Before 50 min, two shoulders at 903 and 1112 cm^{-1} in the spectra of APP1 solution were caused by the asymmetric stretching vibration of the P−O−P structure and the P−OH structure in $H_2P_3O_{10}^{3-}$, respectively.[34] As shown in Figure 6b, the intensity of the band between 900 and 1200 cm^{-1} was significantly increased for more dissolving of MAP.[35] A new shoulder near 1132 cm^{-1} was attributed to much NH_4^+ causing symmetric vibration from the ≡M−PO^{3-} structure,[36] where M usually refers to a metal cation, and the signal generated here may be due to the presence of NH_4^+. Figure 6c compares the spectral results collected at 20 min and 135 min, and it can be seen that with the addition of MAP, the signals of ν_{as}(P−O) and ν_s(P−O) at 935$^-$ and 1068 cm^{-1} were gradually enhanced to mask part of ν_{as}(P−O−P) and ν_{as}(P−OH) signals provided by

https://doi.org/10.1021/acsomega.2c04534
ACS Omega 2022, 7, 35885−35900

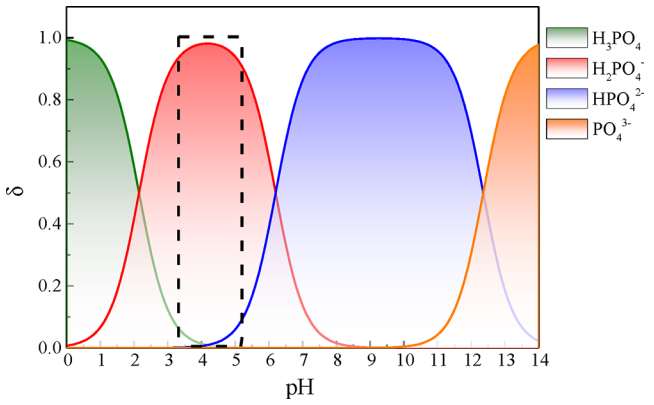

Figure 8. Effect of different pH values on H_3PO_4, $H_2PO_4^-$, HPO_4^{2-}, and PO_4^{3-}.

Table 4. Parameters of the Modified Apelblat Equation for Solubility of MAP with the Addition of APP1[a]

m_1	A	B	C	adj. R^2
0.0000	−3.3793	−1290.6753	2.0669	0.9995
0.0738	0.5023	−1265.7641	1.3777	0.9996
0.1496	7.4477	−1521.4898	0.3125	0.9998
0.2214	6.4440	−1461.9377	0.4567	0.9998
0.2952	3.8078	−1297.7973	0.8248	0.9998
0.3690	7.4963	−1462.8987	0.2778	0.9998
0.4428	6.3498	−1357.5050	0.4193	0.9995
0.5166	3.5834	−1216.1381	0.8232	0.9998
0.5904	−3.7257	−875.5772	1.9074	0.9998
0.6642	−1.2066	−982.3774	1.5313	0.9995
0.7380	0.1234	−1032.7329	1.3310	0.9999
0.8118	−4.1441	−813.0135	1.9520	0.9992
0.8856	−2.8863	−861.1283	1.7617	0.9993

[a] m_1, molality of APP1; A, B, and C, model parameters of the modified Apelblat equation.

APP1. On this basis, according to the ion chromatographic analysis of Figure 6d, it can be seen that the intensity of the P1 peak increased significantly after equilibrium, and the relative intensity of P2, P3, P4, P5, P6, P7, and P8 remained the same as before MAP was added. With the gradual dissolution of MAP, the content of PO_4^{3-} in the liquid phase increased significantly, and the type and relative content of polyphosphate remained almost unchanged. In conclusion, the equilibrium liquid phase is composed of a mixed solution of MAP and APP1 without hydrolysis of polyphosphate. In addition, the solid phase was obtained after the ternary system reached the solid−liquid equilibrium by filtration. The XRD patterns of some of the samples shown in Figure 7a indicated that MAP was still the main form of existence. Meanwhile, the distribution of phosphorus species in solid samples was analyzed by ion chromatography to determine whether there was APP1 residue. As can be seen from Figure 7b, all recovered solid samples mainly contained PO_4^{3-}, indicating that the solid phase did not contain APP1. The extremely slight P2 and P3 signals detected in some samples may be due to the small amount of solution remaining on the solid surface carrying some polyphosphoric ions.

3.2. Effect of APP1 on the Density of Dissolved Equilibrium Solution. In the temperature range of 278.2 and 313.2 K, a series of solution systems with solid−liquid equilibrium were obtained by adding different proportions of APP1. the density of the solutions was measured with a 50 mL density bottle, and the data are shown in Table 3. The density of the solution was positively correlated with the temperature and the amount of APP1, and the maximum density of the solution could reach 1.2811 g/cm^3 (m_1 = 0.8856 mol/kgH_2O, 313.2 K). With the increase of APP1 addition, the solubility of MAP increased, and therefore the solution density increased. At different temperatures, the solubility of MAP increased gradually in a certain range, and the density of the corresponding solution also increased in a certain range with the increase in the solubility of MAP. In addition, at the same temperature, the increase of APP1 addition can promote the increase of solution density, but the higher the temperature, the weaker the promoting effect. It can be calculated that adding 0.8856 mol/kgH_2O APP1 can increase the density of the solution by 9.99% at 278.2 K but only by 6.61% at 313.2 K. In summary, higher temperature and higher amount of APP1 addition could promote more MAP to dissolve in the solution and thus increase its density. At the same temperature, when more APP1 was added, the molality of APP1 and MAP in the corresponding equilibrium solution with higher density increased.

3.3. Effect of APP1 on the pH Value of Dissolved Equilibrium Solution. The pH value of MAP solution with a concentration of 0.1 mol·L^{-1} was 4.0.[37] The equilibrium system was made to stand for 1 h and then filtered. The pH value of the filtrate was measured by a pH meter, and all results are listed in Table 3. It can be analyzed that the change of APP1 addition and temperature can significantly affect the composition of the solution, resulting in the change of its pH value. When APP1 was not added, the MAP solubility increases with the increase of temperature, corresponding to the formation of a higher concentration of MAP solution with a lower pH value. Under the same APP1 addition, the pH value decreased with the increase of temperature, and the maximum pH value was 5.15 (m_1 = 0.8856 mol/kgH_2O, 278.2 K) and the minimum was 3.36 (no APP1, 313.2 K). Higher APP1 addition can promote the dissolution of MAP and lead to the increase of the molality of APP1 and MAP in the solution. However, at the same temperature, the pH of the solution increased with the increase of APP1 addition, which may be because the dissolved $P_nO_{3n+1}^{(n+2)-}$ ions consumed more H^+. Although adding APP1 increased the amount of MAP dissolved, much APP1 dissolving at the same time led to an increase in the pH value. The hydrolysis reaction of APP1 dissolved in the solution was an important reason for the increase in the pH of the solution and the solubility of MAP. As shown in Figure 8, the concentration distributions of H_3PO_4, $H_2PO_4^-$, HPO_4^{2-}, and PO_4^{3-} at different pH values were plotted according to the dissociation constant of phosphoric acid[38] and the database of OLI analyzer 9.6 software platform.[39]

From Figure 8, it can be seen that when MAP and APP1 were codissolved in equilibrium, a solution system with pH of 3.3−5.2 was obtained, and the following reaction equilibrium relationship may exist.

$$NH_4H_2PO_4(s) \rightleftharpoons NH_4^+ + H_2PO_4^- \quad (5)$$

$$H_2O \rightleftharpoons H^+ + OH^- \quad (6)$$

$$NH_4^+ + H_2O \rightleftharpoons NH_3{\cdot}H_2O + H^+ \quad (7)$$

$$H_2PO_4^- \rightleftharpoons H^+ + HPO_4^{2-} \quad (8)$$

https://doi.org/10.1021/acsomega.2c04534
ACS Omega 2022, 7, 35885−35900

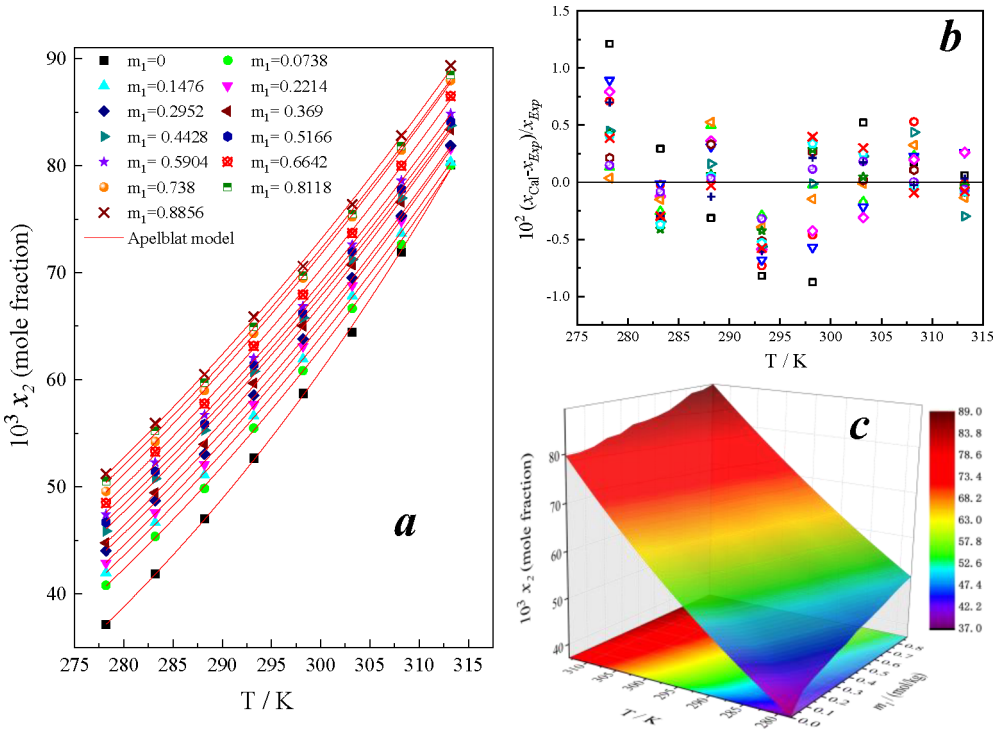

Figure 9. Fitting effect of the modified Apelblat equation on MAP solubility in a mixed system: (a) Fitting curve analysis, (b) relative deviation analysis, and (c) fitting surface analysis.

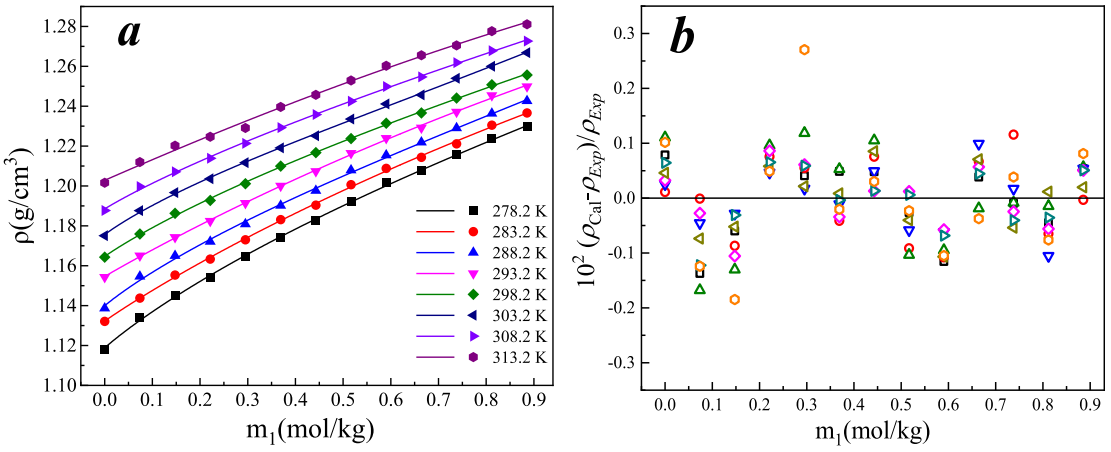

Figure 10. Fitting effect of eq 11 on the density data of the mixed solution: (a) Fitted curve analysis and (b) relative deviation analysis.

Table 5. Regression Coefficients Obtained from Formula 11 to Fit the Density Data of the Ternary System[a]

T/K	a_0	a_1	a_2	a_3	adj. R^2
278.2	1.1188	0.2225	−0.1444	0.0443	0.9993
283.2	1.1322	0.1724	−0.0606	0.0027	0.9991
288.2	1.1399	0.2126	−0.1617	0.0636	0.9983
293.2	1.1546	0.1422	−0.0245	−0.0122	0.9993
298.2	1.1647	0.1751	−0.1092	0.0352	0.9993
303.2	1.1756	0.1925	−0.1721	0.0823	0.9991
308.2	1.1885	0.1538	−0.0898	0.0299	0.9991
313.2	1.2029	0.1036	0.0054	−0.0217	0.9959

[a] a_0, a_1, a_2, and a_3 are the regression coefficients of eq 11.

$$H_2PO_4^- + H^+ \rightleftharpoons H_3PO_4 \quad (9)$$

The pH value of APP1 solution was closer to neutral than that of MAP. The addition of APP1 to MAP solution was accompanied by a certain degree of hydrolysis reaction, and the newly established acid−base equilibrium would promote the reverse reaction of eq 6 so as to increase the pH of the solution. Then, the positive reactions of equilibrium reactions (7) and (8) were promoted, and finally the balance of eq 5 was promoted to the direction of positive reaction to increase the solubility of MAP.

3.4. Model and Parameterization. *3.4.1. Simulation and Parameterization of Solubility. 3.4.1.1. Modified Apelblat Equation.* The simplified Apelblat model is a commonly used semiempirical equation following fundamental principles of solid−liquid equilibrium.[40] It was used for the regression analysis of the experimental solubility data of MAP obtained to get reliable modeling parameters. When the solution reaches solid−liquid equilibrium, the solids in the solution system can

https://doi.org/10.1021/acsomega.2c04534
ACS Omega 2022, 7, 35885−35900

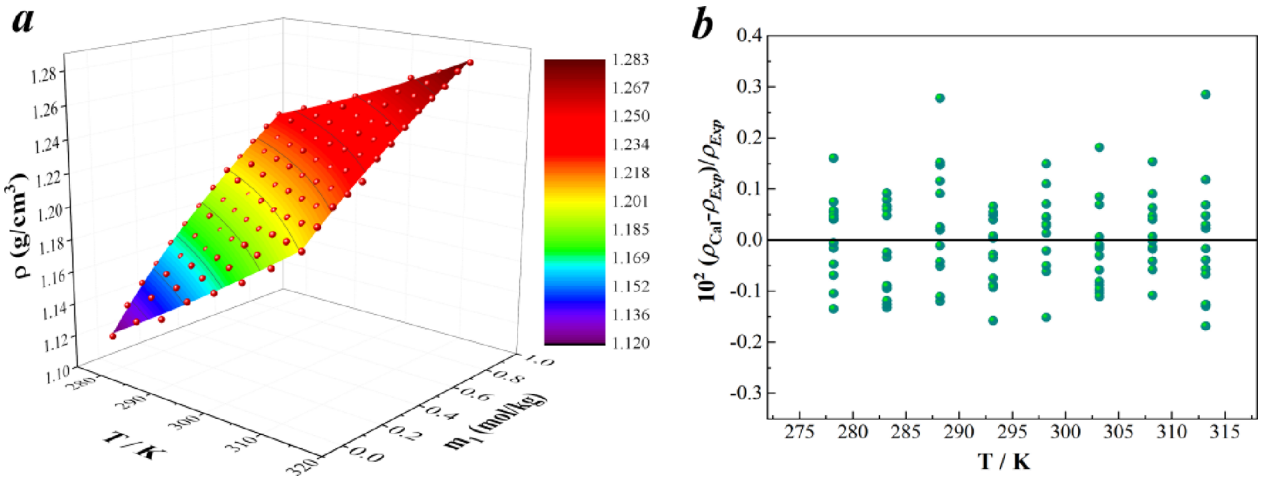

Figure 11. Fitting effect of eq 12 on the density data of the mixed solution: (a) Analysis of 3D surface fitting and (b) relative deviation analysis.

Table 6. Regression Coefficients Obtained from Formula 12 to Fit the Density Data of the Ternary Solution (MAP Saturated)[a]

para.	values
k_1	−0.001380
k_2	6.830×10^{-6}
k_3	2.432
k_4	0.07700
k_5	-1.140×10^{-9}
k_6	−0.007200
k_7	1.340×10^{-5}
k_8	1.151
adj. R^2	0.9991

[a] k_1, k_2, k_3, k_4, k_5, k_6, k_7, and k_8 are the regression coefficients of eq 12.

no longer enter the liquid. The effect of heat tolerance was negligible in the experimental temperature range, and ΔH_m can be regarded as a constant value. The temperature of the triple point was considered to be close to the melting point of the solid under atmospheric pressure, and the temperature of the melting point was used to replace the temperature of the triple point. The Apelblat model can be further simplified as

$$\ln x_2 = A + \frac{B}{T} + C \ln T \tag{10}$$

where A, B, and C are the model parameters of this equation.

3.4.1.2. Solubility Model Parameterization. The experimental data were analyzed by a simplified Apelblat model with

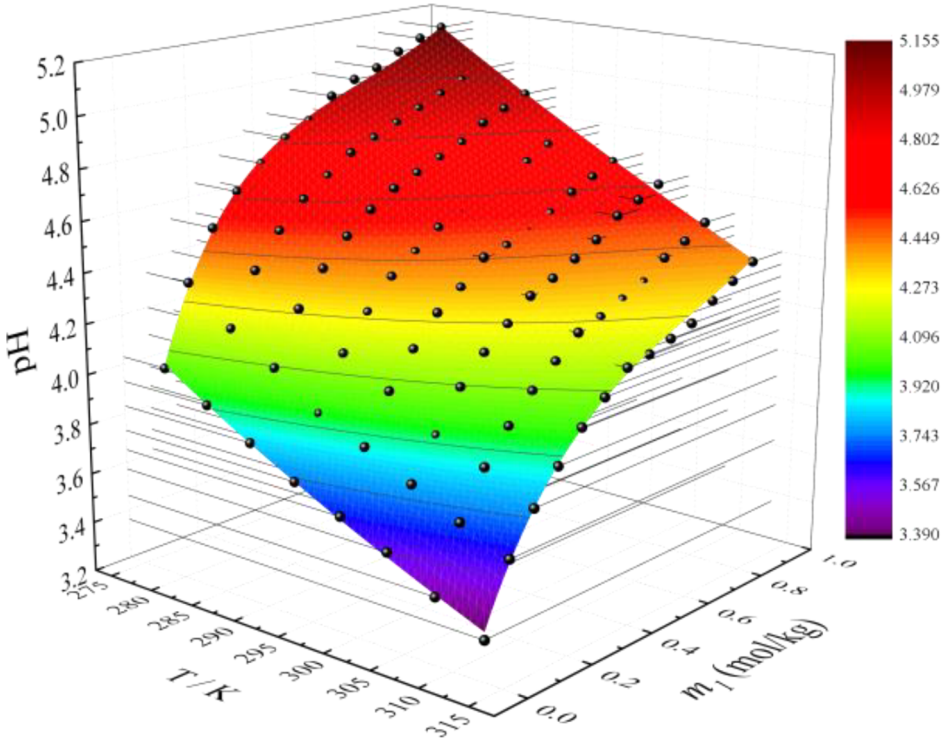

Figure 12. 3D surface fitting diagram of the pH values of MAP-saturated mixed solution (APP1−MAP−water) using Rational 2D models; m_1 represents the mass molality of APP1.

https://doi.org/10.1021/acsomega.2c04534
ACS Omega 2022, 7, 35885−35900

Table 7. Parameters of the Rational 2D Model for the pH Values of Ternary Solution[a]

parameters	value
A_0	−548.2
A_1	2.764
A_2	−0.4839
A_3	0.002000
A_4	1.641×10^{-6}
B_1	619.3
B_2	−425.1
B_3	124.0
B_4	91.11
B_5	−43.35
adj. R^2	0.9983

[a] A_0, A_1, A_2, A_3, A_4 and B_1, B_2, B_3, B_4, B_5 are the regression coefficients of eq 13.

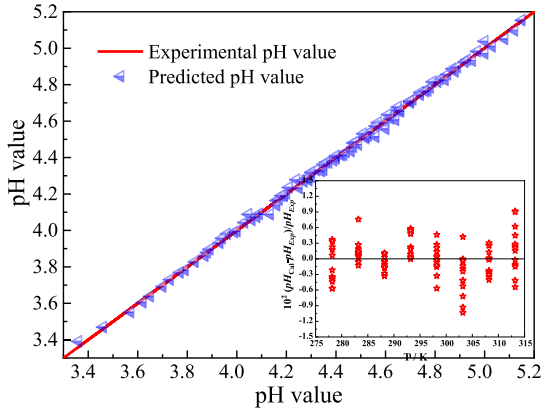

Figure 13. Correlation between the experimental pH value and the predicted pH value in ternary APP1−MAP−water solution (MAP saturated).

the corresponding model parameters shown in Table 4 and the fitting effect and residual analysis are depicted in Figure 9.

As can be seen from Figure 9a, within the measured temperature range, the simplified Apelblat model can be used to reliably express the change trend of the solubility of MAP after APP1 was added. From Figure 9b, the relative deviations between the fitting data and experimental data were all less than 1.25%, and the largest deviation occurred in the fitting value of MAP solubility in pure water, which was 1.21%. The small deviation between the fitted results and the actual values indicates that the model can reliably describe the dissolution equilibrium law of the system. Moreover, it can be seen in Table 4 that the correlation coefficient (R^2) values obtained were all greater than 0.9990, indicating the accuracy of fitting results. In addition, we summarized the data of the fitting curve and plotted the 3D fitting surface, as shown in Figure 9c. This 3D surface can simultaneously show the joint effect of temperature and APP1 addition on MAP solubility and play a good role in predicting and judging the practical application. From the data results at 313.2 K in Figure 9c, it can be clearly seen that the fitting results provided reliable data fluctuation and change rules, which also reaffirmed the value of this model.

3.4.2. Simulation and Parameterization of Density. The density of common inorganic salt aqueous solutions is mostly a function of concentration at a certain temperature. In this study, two polynomial models were used to fit the density changes of the ternary equilibrium system. The following polynomials were reported by Gucker et al[41]

$$\rho = a_0 + a_1 m + a_2 m^{1.5} + a_3 m^2 \quad (11)$$

where m is the concentration of solution, mol/kgH_2O. In this work, m represents the concentration of APP1 and a_0, a_1, a_2, and a_3 are the regression coefficients. In addition, Zeng proposed an 8-parameter empirical equation that can fully consider the effects of concentration and temperature and their interactions on solution density.[42]

$$\rho = (\rho_0 + k_1 m + k_2 m^2 + k_3 T + k_4 T^2 + k_5 m^3 + k_6 mT + k_7 m^2 T)/(1 + k_8 T) \quad (12)$$

In this formula, ρ_0 represents the density of water or the density of reference solution at 273.2 K; k_i is a regression parameter; T means the temperature of the solution; m refers the molality of APP1 in this work. Equations 11 and 12 are used to fit the experimental data of density. The fitting results and relative deviation of formula 11 are shown in Figure 10, and the corresponding regression parameters are listed in Table 5. The fitting effect and related parameters of eq 12 are shown in Figure 11 and Table 6 respectively.

As can be seen from Figure 10a, the fitting curve obtained by using the polynomial eq 11 was in good agreement with the experimental data points. As shown in Figure 10b, the relative deviation between the fitting value and the experimental value was all within 0.30%. From Table 5, the average correlation coefficients (R^2) of the density data were greater than 0.99. The polynomial eq 11 can be used to reliably describe the changing trend of the ternary mixed solution density with different APP1 additions.

As shown in Figure 11a, the fitting results of the density of MAP solution using formula 12 were reliable enough to predict the density of ternary solution under different conditions. From Table 6 and Figure 11b, it can be seen that the correlation coefficient (R^2) of the fitting curve was greater than 0.99, and the relative deviation was less than 0.30%. Therefore, the fitting results of the two models both had high correlation coefficients and small deviation, and they can be used together to improve accuracy and reliability.

3.4.3. Simulation and Parameterization of pH Value. Rational 2D function in the Origin software was used to fit the change of pH value of ternary solution (MAP saturated) with different APP1 additions.[43]

$$\mathrm{pH} = \frac{A_0 + A_1 t + B_1 m + B_2 m^2 + B_3 m^3}{1 + A_2 t + A_3 t^2 + A_4 t^3 + B_4 m + B_5 m^2} \quad (13)$$

where A_0, A_1, A_2, A_3, A_4 and B_1, B_2, B_3, B_4, B_5 are model parameters and m is the mass molality of APP1. The pH values measured and the fitting results by Rational 2D function are drawn in Figure 12. The corresponding regression parameters are summarized in Table 7, and relative deviation analysis between the experimental value and the fitted value is shown in Figure 13.

As can be seen from Figure 12, under the same APP1 addition, the pH value of the solution decreased with temperature, and the maximum value can reach 5.15 (m_1 = 0.8856 mol/kgH_2O, 278.2 K). At each temperature, the pH value of the solution increased with the increasing addition of APP1, and the minimum value was 3.36 (m_1 = 0 mol/kgH_2O, 313.2 K). From Figure 13, the experimental data points were almost all on the diagonal and

https://doi.org/10.1021/acsomega.2c04534
ACS Omega 2022, 7, 35885−35900

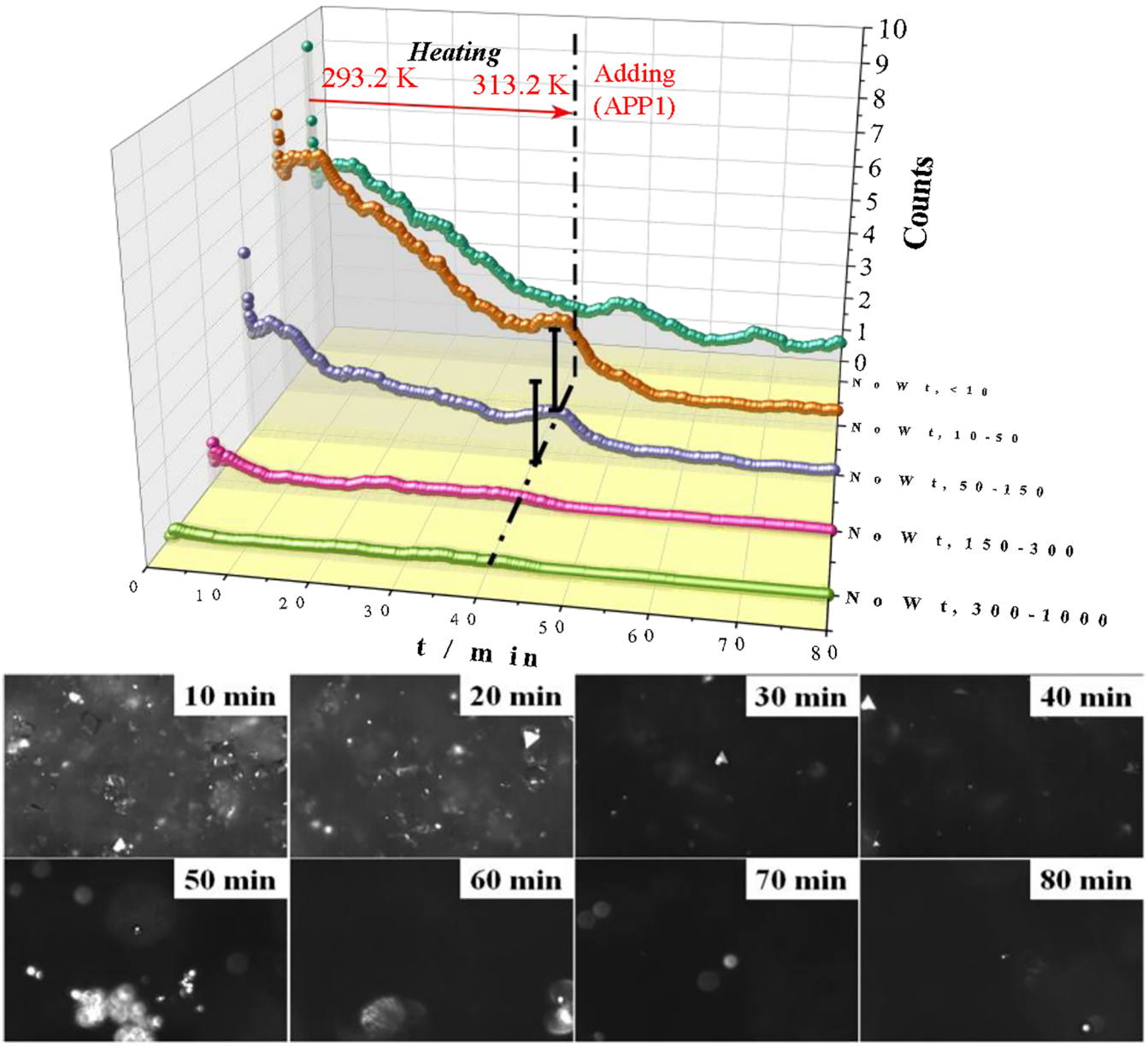

Figure 14. Online detection technology monitoring the dissolution process of APP1−MAP−water system.

their relative deviations were all within 0.1%, indicating that the Rational 2D function can reliably predict the pH value of ternary solution.

3.5. On-Line Monitoring of Mixed Dissolution Behavior. Based on experimental data, the solubility of MAP increased from 4.8342 to 5.5373 mol/kg after APP1 (0.8856 mol/kgH_2O) was added at 313.2 K. First, we carried out the simulation verification experiment in 500 mL of water and weighed 318.8205 g of MAP according to the maximum solubility of MAP that could be achieved by adding 0.8856 mol/kgH_2O APP1 at 313.2 K. At 293.2 K, 318.8205 g of MAP was added in 500.04 mL of water to form a simulated supersaturated solution. At this time, undissolved MAP existed in the system in the form of particles which could be detected by FBRM. The changes in the chord length and the number of MAP particles during subsequent heating and APP1 addition were recorded by FBRM. Then, the temperature of the dissolved system was increased from 293.2 to 313.2 K at a rate of 2 K/min. When the temperature reached 313.2 K, the system was still in the supersaturated state because the saturated dissolved amount of MAP was still lower than the added amount. When the particle signal observed by FBRM remained stable, 119.9988 g of APP1 (~0.8856 mol/kgH_2O) was added to the system at one time. The purpose of this experiment was to reverse verify that APP1 can promote MAP dissolution with the help of an online particle observation system. The particle changes in the whole process were monitored in real time using FBRM and PVM, and the results are shown in Figure 14.

From Figure 14, the change curve of the particle number in different chord length ranges reflects the variation of particle size in the system. A heating process of 293.2−313.2 K was experienced in the reactor in 10−20 min, the solubility of MAP in the system increased, more MAP crystals dissolved gradually, and the chord length curves all showed a downward trend. Until 30 min later, the curve gradually tends to level and the system reaches a new supersaturated state, and there are still incomplete dissolved MAP particles. After 40 min, when APP1 was added to the system, the chord length curves showed a further downward

https://doi.org/10.1021/acsomega.2c04534
ACS Omega 2022, 7, 35885−35900

trend. This process was due to the reduction of particle number caused by the dissolution of APP1 and undissolved MAP. After 70 min, the number of particles in the system decreased to a minimum and this state maintained for 10 min, indicating that the particles in the system no longer changed. Only 1.6 particles with a size smaller than 10 μm and 0.4 particles with a size in the range of 10−50 μm existed. It was possible that the inadequately cleaned probe and impurities caused errors, so that not all curves coincided with the *X*-axis. Therefore, we approximately regarded that this ternary system equilibrium reached at 80 min. The particle dissolution process detected by FBRM confirmed that APP1 could dissolve in supersaturated MAP solution and promote the continued dissolution of undissolved MAP particles. Moreover, microscopic images of the system were collected by PVM every 10 min. It can be seen that the large-grained crystals in the picture from 10 to 20 min gradually decreased, which was due to the increase of MAP solubility as the temperature increased. After 40 min, a large number of small spherical particles (APP1) appeared in the picture first, and then the particles in the picture gradually decreased to almost nothing until 80 min. This indicated that the particle number reduction phenomenon detected by FBRM after 40 min was also captured by PVM. Thus, the PVM was like a camera that took real pictures in real time to demonstrate the reliability of FBRM. We innovatively verified the dissolution equilibrium law of APP1−MAP−water system with the help of FBRM and PVM and also hoped to provide an application idea of FBRM and PVM.

3.6. Mixed Strategy on Fertilizer Application. APP1 and MAP were both good phosphate fertilizer materials and had their own product advantages. The development of their hybrid formulation is a potential advantage strategy that not only provided both fast-release and slow-release phosphorus but also improved solubility to save irrigation water. In consideration of cost and fertilizer efficiency, this study focused on the system in which P_2O_5 provided by APP1 was less than 30% of the total P_2O_5 content. Within the research scope, the phosphorus contents of the same amount of MAP saturated solutions with or without APP1 were compared and are shown in Table S3. They can be synergistically codissolved to increase the concentration of phosphorus in the solution to reduce irrigation water, and the formula can be adjusted to provide different phosphorus contents. This study also opened up ideas and built a certain data foundation for expanding the application scheme of new phosphate fertilizer products.

4. CONCLUSIONS

In the ternary APP1−MAP−water mixed solution system, the pH and density of the ternary equilibrium solution and solubility data of $NH_4H_2PO_4$ were obtained under different APP1 additions and temperatures. At each temperature, the density and pH of ternary solution increased with APP1 addition. Under the same APP1 concentration, the solubility of MAP and the density of the solution increased with temperature, while the pH value decreased. The increase of MAP solubility was positively correlated with the increase of APP1 addition and temperature, and the increase of temperature had a stronger promoting effect. The simplified Apelblat model, the empirical polynomial, and the Rational 2D function were used to express the solubility data of MAP, density value, and pH values, respectively. The fitting values of these models all showed good consistency (R^2 > 0.9900) with the experimental data. Moreover, FBRM and PVM were used to continuously monitor the codissolution process of APP1 and MAP, and it was found that APP1 can further promote the complete dissolution of MAP supersaturated solution within 40 min. All phase equilibrium conclusions and parametric models provided in this study can assist these two phosphate fertilizer materials to play a better synergistic role in the mixed irrigation process. More experiments would be carried out to explore the effect of the adding order on the dissolution process to find an optimal mixing scheme. Subsequent studies should develop mixed formulations for specific crops based on theoretical data and explore long-term advantages of mixed strategies compared with traditional fertilization programs. The application evaluation of the mixed formula should be improved through pot experiment and field amplification.

■ ASSOCIATED CONTENT

Supporting Information

The Supporting Information is available free of charge at https://pubs.acs.org/doi/10.1021/acsomega.2c04534.

Description of uncertainty evaluation method; comparison analysis between experimental results and available literature data; comparison of MAP solubility data; comparison of the MAP solution density data; graphical presentation of literature and experimental data; research practical significance introduction; analysis of P_2O_5 content in a mixed solution system of APP1 and MAP; introduction of real-time online particle analysis technology; probe structure and optical measurement principle of FBRM; chord length of particles measured by FBRM in the system; and application of on-line monitoring system in a practical experiment (PDF)

■ AUTHOR INFORMATION

Corresponding Author

Xinlong Wang − *Ministry of Education Research Center for Comprehensive Utilization and Clean Processing Engineering of Phosphorus Resources, School of Chemical Engineering, Sichuan University, Chengdu 610065, PR China;* orcid.org/0000-0002-5279-5859; Email: wangxl@scu.edu.cn

Authors

Xiaohou Zhou − *Ministry of Education Research Center for Comprehensive Utilization and Clean Processing Engineering of Phosphorus Resources, School of Chemical Engineering, Sichuan University, Chengdu 610065, PR China;* orcid.org/0000-0001-5128-1082

Dejun Xu − *Ministry of Education Research Center for Comprehensive Utilization and Clean Processing Engineering of Phosphorus Resources, School of Chemical Engineering, Sichuan University, Chengdu 610065, PR China*

Dehua Xu − *Ministry of Education Research Center for Comprehensive Utilization and Clean Processing Engineering of Phosphorus Resources, School of Chemical Engineering, Sichuan University, Chengdu 610065, PR China;* orcid.org/0000-0001-5385-9968

Zhengjuan Yan − *Ministry of Education Research Center for Comprehensive Utilization and Clean Processing Engineering of Phosphorus Resources, School of Chemical Engineering, Sichuan University, Chengdu 610065, PR China;* orcid.org/0000-0002-8583-8173

Zhiye Zhang − *Ministry of Education Research Center for Comprehensive Utilization and Clean Processing Engineering*

https://doi.org/10.1021/acsomega.2c04534
ACS Omega 2022, 7, 35885−35900

of Phosphorus Resources, School of Chemical Engineering, Sichuan University, Chengdu 610065, PR China

Benhe Zhong − *Ministry of Education Research Center for Comprehensive Utilization and Clean Processing Engineering of Phosphorus Resources, School of Chemical Engineering, Sichuan University, Chengdu 610065, PR China*

Complete contact information is available at: https://pubs.acs.org/10.1021/acsomega.2c04534

Notes

The authors declare no competing financial interest.

■ ACKNOWLEDGMENTS

X.W., X.Z., B.Z., Z.Z., D.X., and D.X. received funding from the National Natural Science Foundation of China (Project No. :32172677). X.W., X.Z., B.Z., Z.Z., D.X., and D.X. received funding from the National Key Research and Development Program of China (Project No. 2018YFC1900202). Z.Y. and D.X. received funding from the Sichuan Science and Technology Program (Project No. 2018RZ0145). The authors gratefully thank for the support and assistance for the OLI System platform V9.6 in simulation computing.

■ NOMENCLATURE

MAP	monoammonium phosphate
APP	ammonium polyphosphate
T	absolute temperature of dissolved system
P	absolute pressure of the experimental environment
x_1	molar fraction of APP1
x_2	molar fraction of MAP
m_1, m_2	molarities of APP1 and MAP
WAP	average polymerization by weight
NAP	number average degree of polymerization
PR	polymerization rate
PDI	polymer dispersity index
Pn	polyphosphate ions of different polymerization degrees ($P_nO_{3n+1}^{(n+2)-}$)
m_0	mass of water added
m_1	mass of water-soluble APP1 added in ternary system
m_2	mass of MAP added in ternary system
M_0	molar mass of water
M_1	molar mass of APP1
M_2	molar mass of MAP
ρ	density of dissolved system
OT	ratio of orthophosphate phosphorus content to total phosphorus content in the liquid phase at equilibrium state
XRD	X-ray diffractometer
R	ideal gas constant, 8.314 $J{\cdot}mol^{-1}{\cdot}K^{-1}$
a, b	model parameters of activity coefficient
ΔH_m	melting enthalpy
A, B, and C	model parameters of Apelblat model
k_1, k_2, k_3, k_4, k_5, k_6, k_7, k_8	regression parameters of density fitting equation
A_0, A_1, A_2, A_3, A_4 and B_1, B_2, B_3, B_4, B_5	parameters of Rational 2D function

■ REFERENCES

(1) Cichy, B.; Folek, S. Utilization of complexing abilities of polyphosphates in liquid fertilizers, based on the example of fertilizer type NP and type NPK with zinc. *Ind. Eng. Chem. Res.* **2005**, *44*, 4513−4517.

(2) Yang, J. X.; Kong, X. J.; Xu, D. H.; Xie, W. J.; Wang, X. L. Evolution of the polydispersity of ammonium polyphosphate in a reactive extrusion process: Polycondensation mechanism and kinetics. *Chem. Eng. J.* **2019**, *359*, 1453−1462.

(3) Yang, J. X.; Xie, W. J.; Kong, X. J.; Xu, D. H.; Wang, X. L. Reactive extrusion of ammonium polyphosphate in a twin-screw extruder: polydispersity improvement. *Chem. Eng. Process.* **2018**, *133*, 58−65.

(4) Hossner, L. R.; Freeouf, J. A. Acidic ammonium polyphosphate fertilizer as carriers for manganese. *J. Agric. Food Chem.* **1973**, *21*, 705−707.

(5) Hill, M. W.; Hopkins, B. G.; Jolley, V. D.; Webb, B. L. Phosphorus Mobility Through Soil Increased with Organic Acid-Bonded Phosphorus Fertilizer (Carbond P). *J. Plant Nutr.* **2015**, *38*, 1416−1426.

(6) Venugopalan, M. V.; Prasad, R. Relative efficiency of ammonium polyphosphate and orthophosphates for wheat and their residual effects on succeeding cowpea fodder. *Fert. Res.* **1989**, *20*, 109−114.

(7) Xie, W.-J.; Wang, X.-L.; Li, Y.-S.; Xu, D.-H.; Zhong, Y.-J.; Yang, J.-X. Simultaneous determination of various phosphates in water-soluble ammonium polyphosphate. *Chromatographia* **2019**, *82*, 1687−1695.

(8) Gao, Y.; Kang, L.; Chu, G. Effects of polyphosphate fertilizers with different polymerization degrees and polymerization rates on the availability of phosphorus and trace elements in calcareous soils. *Zhiwu Yingyang Yu Feiliao Xuebao* **2018**, *24*, 1294−1302. From Cnki

(9) Chen, X.; Yang, Y.; Gong, L.; Zhang, C. Effect of distance of seed-fertilizer co-sowing ammonium polyphosphate on seedling growth of maize. *Linfei Yu Fufei* **2018**, *33*, 37−40. From Cnki

(10) Xiang, Y.; Ru, X.; Shi, J.; Song, J.; Zhao, H.; Liu, Y.; Zhao, G. Granular, Slow-Release Fertilizer from Urea-formaldehyde, Ammonium Polyphosphate, and Amorphous Silica Gel: A New Strategy Using Cold Extrusion. *J. Agric. Food Chem.* **2018**, *66*, 7606−7615.

(11) Xu, D. H.; Xiong, X.; Xu, D. J.; Zhong, Y. J.; Wang, X. L.; Zhang, Z. Y.; Yang, X. S. Experimental determination of solubility and metastable zone width of ammonium dihydrogen phosphate in (NH 4) 2 SO 4 + water and NH 4 F + water systems. *Fluid Phase Equilib.* **2018**, *468*, 1−8.

(12) Yang, Z. P.; Li, J.; Luo, J. H.; Wang, P.; Zhou, K. Solid-liquid phase equilibrium for the ternary system urea phosphate+ammonium dihydrogen phosphate+water at 25 and 55°C. *Fluid Phase Equilib.* **2012**, *335*, 60−63.

(13) Srinivasan, K.; Anbukumar, S.; Ramasamy, P. Mutual solubility and metastable zone width of $NH_4H_2PO_4$-KH_2PO_4 mixed-solutions

and growth of mixed-crystals. *J. Cryst. Growth* **1995**, *151*, 226−229. Letter
(14) Zhumaniyazov, M. Z.; Beglov, B. M.; Khodzhaev, O. F.; Yuldashev, N. K. Solubility polytherm of the ternary system hexamethylenetetramine-ammonium dihydrogen phosphate-water. *Russ. J. Gen. Chem.* **2004**, *74*, 1001−1004.
(15) Yang, X. Y.; Fang, S. B. Practices, perceptions, and implications of fertilizer use in East-Central China. *Ambio* **2015**, *44*, 647−652.
(16) Kamat, D. R.; Savant, V. V.; Sathyanarayana, D. N. A rapid and highly selective method for the estimation of pyro-, tri- and orthophosphates. *Talanta* **1995**, *42*, 365−373.
(17) Xie, W. J.; Wang, X. L.; Li, Y. S.; Xu, D. H.; Zhong, Y. J.; Yang, J. X. Simultaneous Determination of Various Phosphates in Water-Soluble Ammonium Polyphosphate. *Chromatographia* **2019**, *82*, 1687−1695.
(18) McBeath, T. M.; Lombi, E.; McLaughlin, M. J.; Bünemann, E. K. Polyphosphate-fertilizer solution stability with time, temperature, and pH. *J. Plant Nutr. Soil Sci.* **2007**, *170*, 387−391.
(19) Gao, Y. J.; Wang, X. W.; Shah, J. A.; Chu, G. X. Polyphosphate fertilizers increased maize (Zea mays L.) P, Fe, Zn, and Mn uptake by decreasing P fixation and mobilizing microelements in calcareous soil. *J. Soils Sediments* **2020**, *20*, 1−11.
(20) Venugopalan, M. V.; Prasad, R. Relative efficiency of ammonium polyphosphate and orthophosphates for wheat and their residual effects on succeeding cowpea fodder. *Fert. Res.* **1989**, *20*, 109−114.
(21) Xie, W.; Wang, X.; Xu, D.; Liang, W.; Lin, H.; Leng, X.; Yang, J. Effect of different pH on the hydrolysis of ammonium pyrophosphate. *Wujiyan Gongye* **2019**, *51*, 28−31. From Cnki
(22) Wang, L.; Gong, L.; Deng, L.; Tu, P.; Yang, Y.; Guan, L.; Chen, F.; Zhang, C. Effect of different temperature and pH on the hydrolysis of ammonium polyphosphate. *Linfei Yu Fufei* **2015**, *30*, 8−11. From Cnki
(23) Zhou, X. H.; Zheng, W. J.; Xu, D. H.; Luo, T.; Zhang, Z. Y.; Wang, X. L. Solubility measurement and thermodynamics modelling for potassium dihydrogen phosphate in a water-ethanol system from 293.2 to 323.2 K. *Fluid Phase Equilib.* **2020**, *512*, 112533.
(24) Sodhi, I.; Mallepogu, P.; Thorat, V. P.; Kashyap, M. C.; Sangamwar, A. T. Insights on role of polymers in precipitation of celecoxib from supersaturated solutions as assessed by focused beam reflectance measurement (FBRM). *Eur. J. Pharm. Sci.* **2019**, *137*, 104983.
(25) Kutluay, S.; Ceyhan, A. A.; Şahin, O.; İzgi, M. S. Utilization of In Situ FBRM and PVM Probes to Analyze the Influences of Monopropylene Glycol and Oleic Acid as Novel Additives on the Properties of Boric Acid Crystals. *Ind. Eng. Chem. Res.* **2020**, *59*, 9198−9206.
(26) Zhao, J.; Wang, M. L.; Dong, B. L.; Feng, Q.; Xu, C. X. Monitoring the Polymorphic Transformation of Imidacloprid Using in Situ FBRM and PVM. *Org. Process Res. Dev.* **2013**, *17*, 375−381.
(27) Xu, D. J.; Xiong, X.; Yang, L.; Zhang, Z. Y.; Wang, X. L. Determination of the Solubility of Ammonium Dihydrogen Phosphate in Water-Ethanol System at Different Temperatures from 283.2 to 343.2 K. *J. Chem. Eng. Data* **2016**, *61*, 78−82.
(28) Buchanan, G. H.; Winner, G. B. The Solubility of Mono- and Diammonium Phosphate. *J. Ind. Eng. Chem.* **1920**, *12*, 448−451.
(29) He, T.; Sun, J.; Shen, W.; Ren, Y. Solid-liquid phase equilibria of quaternary system $NH_4^+//C1^{(-)}$, SO_4^{2-}, $H_2PO_4^-$-H_2O and its subsystems. $NH_4^+//C1^{(-)}$, SO_4^{2-}-H2O, $NH_4^+//C1^{(-)}$, $H_2PO_4^-$-H_2O at 313.15 K. *J. Chem. Thermodyn.* **2017**, *112*, 31−42.
(30) Mishra, A. K.; Ahluwalia, J. C. Apparent molal volumes of amino acids, N-acetylamino acids, and peptides in aqueous solutions. *J. Phys. Chem.* **1984**, *88*, 86−92.
(31) Kumar, H.; Behal, I. Densities and Speeds of Sound of Solutions of Glycine, L-Alanine, and L-Valine in Aqueous Ammonium Dihydrogen Phosphate at Different Temperatures. *J. Chem. Eng. Data* **2017**, *62*, 3138−3150.
(32) Kumar, H.; Behal, I.; Siraswar, S. Densities and Speeds of Sound for Sucrose in Aqueous Solutions of Ammonium Phosphate Salts at Different Temperatures through Density and Speed of Sound Measurements. *J. Chem. Eng. Data* **2019**, *64*, 3772−3780.
(33) Kumar, H.; Kumar, V.; Sharma, S.; Katal, A.; Alothman, A. A. Volumetric and acoustic properties of amino acids L-Leucine and L-Serine in aqueous solution of ammonium dihydrogen phosphate (ADP) at different temperatures and concentrations. *J. Chem. Thermodyn.* **2021**, *155*, 106350.
(34) Kazmierczak-Razna, J.; Nowicki, P.; Wiśniewska, M.; Nosal-Wiercińska, A.; Pietrzak, R. Thermal and physicochemical properties of phosphorus-containing activated carbons obtained from biomass. *J. Taiwan Inst. Chem. Eng.* **2017**, *80*, 1006−1013. Puziy, A. M.; Poddubnaya, O. I.; Martínez-Alonso, A.; Suárez-García, F.; Tascón, J. M. D. Synthetic carbons activated with phosphoric acid. *Carbon* **2002**, *40*, 1493−1505. Bourbigot, S.; Le Bras, M.; Delobel, R.; Bréant, P.; Trémillon, J. M. Carbonization mechanisms resulting from intumescence-part II. Association with an ethylene terpolymer and the ammonium polyphosphate-pentaerythritol fire retardant system. *Carbon* **1995**, *33*, 283−294. Guo, Y. P.; Rockstraw, D. A. Physicochemical properties of carbons prepared from pecan shell by phosphoric acid activation. *Bioresour. Technol.* **2007**, *98*, 1513−1521.
(35) Liou, T. H. Development of mesoporous structure and high adsorption capacity of biomass-based activated carbon by phosphoric acid and zinc chloride activation. *Chem. Eng. J.* **2010**, *158*, 129−142.
(36) Guan, X. H.; Liu, Q.; Chen, G. H.; Shang, C. Surface complexation of condensed phosphate to aluminum hydroxide: An ATR-FTIR spectroscopic investigation. *J. Colloid Interface Sci.* **2005**, *289*, 319−327.
(37) Babenko, A. M.; Andrianov, A. M. Solubility in the systems diammonium phosphate ammonium-nitrate potassium-sulfate water and ammonium-nitrate potassium-sulfate water. *Russ. J. Appl. Chem.* **1984**, *57*, 1777−1781.
(38) Dean, J. A. *Langley Chemistry Handbook*; Science Press, 2003.
(39) Zhang, Y.; Li, Z. B.; Asselin, E. Determination and chemical modeling of the solubility of FeSO 4 ·7H 2 O in the Ti(SO 4) 2 −H 2 SO 4 −H 2 O system. *J. Chem. Thermodyn.* **2016**, *102*, 219−227.
(40) Li, H.; Liu, J.; Zhu, J.; Zhao, L.; Wang, H. K.; Zhang, Y. D. Correlation and comparison for solubility of pimelic acid in different solvents. *Russ. J. Phys. Chem. A* **2012**, *86*, 314−316.
(41) Gucker, F. T.; Chernick, C. L.; Roy-Chowdhury, P. A FREQUENCY-MODULATED ULTRASONIC INTERFEROMETER: ADIABATIC COMPRESSIBILITY OF AQUEOUS SOLUTIONS OF N A C L AND KC L AT 25°C. *Proc. Natl. Acad. Sci. U.S.A.* **1966**, *55*, 12−19.
(42) Zeng, Q. S. The density formula of saline aqueous solution. *Huagong Sheji* **1994**, *05*, 35−36. CNKI:SUN:HGSJ.0.1994-05-008
(43) Hochman, A.; Leviatan, Y.; White, J. K. On the use of rational-function fitting methods for the solution of 2D Laplace boundary-value problems. *J. Comput. Phys.* **2013**, *238*, 337−358.

https://doi.org/10.1021/acsomega.2c04534
ACS Omega 2022, 7, 35885−35900